Orientation Modulation for Data Hiding in Clustered-Dot Halftone Prints

Orhan Bulan, *Student Member, IEEE*, Gaurav Sharma, *Senior Member, IEEE*, and Vishal Monga, *Member, IEEE*

***Abstract*—We present a new framework for data hiding in images printed with clustered dot halftones. Our application scenario, like other hardcopy embedding methods, encounters fundamental challenges due to extreme bilevel quantization inherent in halftoning, the stringent requirements of image fidelity, and other unavoidable printing and scanning distortions. To overcome these challenges, while still allowing for automated extraction of the embedded data and a high embedding capacity, we propose a number of innovations. First, we perform the embedding jointly with the halftoning by employing an analytical halftone threshold function that allows steering of the halftone spot orientation within each halftone cell based upon embedded data. In this process, image fidelity is emphasized and, if necessary, the capability to recover individual data values is sacrificed resulting in unavoidable erasures and errors. To overcome these and other sources of errors, we propose a suitable data detection and error control methodology based upon a statistical representation for the print-scan channel that effectively models the channel dependence upon the cover image gray-level. To combat the geometric distortion inherent in the print-scan process, we exploit the periodic halftone structure to recover from global scaling and rotation and propose a novel decision directed synchronization technique that counters locally varying printing distortion. Experimental results demonstrate the power of the proposed framework: we achieve high operational rates while preserving halftone image quality.**

***Index Terms*—Clustered-dot halftones, data hiding, dot orientation modulation, hardcopy data hiding, print-scan channel model.**

I. Introduction

TECHNIQUES for embedding information in hardcopy prints are useful in a wide variety of applications. Document authentication, tamper prevention and detection, meta-data embedding, tracking/inventory control, and entertainment/novelty imaging are examples of applications for which hardcopy data embedding is currently employed. Methods for embedding data in hardcopy prints can be categorized as *data encoding* or *data hiding* approaches. For methods in the former category, data is embedded in a region that is solely dedicated to the objective of conveying the message and the visual appearance of the encoded region is only of secondary concern. One and 2-D barcodes [3]–[5] and DataGlyphs [6], [7] are the predominant representatives of techniques in this class. Data hiding methods, on the other hand, carry the information in a manner that minimally disrupts the primary content included in the print. Various instantiations of print data hiding techniques have also been proposed [8]–[16]. The choice between encoding and hiding methods as well as the type of information embedded and method employed for extraction, depend upon the specific type of the application. In a number of hardcopy data embedding applications, data hiding techniques are particularly attractive because data is embedded within the content and readily incorporated in existing infrastructure. Furthermore, several hardcopy applications mandate high capacity and automated (as opposed to visual, for instance) extraction of the data from a scan of the printed image [17].

From a technical standpoint, adapting a data hiding scheme to the channel characteristics can offer significant performance improvements in terms of robustness and embedding rates [18]. This viewpoint indicates that hardcopy data hiding schemes that aim at high embedding rates and robustness to the print-scan process must specifically adapt to the characteristics of the print-scan channel distortion. The key component of the printing process is a bit-depth reduction step called digital halftoning which produces an illusion of continuous tone (contone) by trading off amplitude resolution for spatial resolution [19]–[21]. Halftone images are typically binary images in which each pixel is either on or off, determining whether ink/toner is deposited on the pixel or not, respectively. Several different halftoning algorithms are utilized in practice and choices among these are made based upon the characteristics of the physical[1] printing process employed in the printer [20]–[22]. For the hardcopy data hiding problem, the channel distortions are intimately tied to the nature of the halftoning algorithm.

In this paper, we propose a method for data hiding in images printed using clustered-dot halftoning, which is the primary

Manuscript received December 04, 2008; revised March 08, 2010. First published March 29, 2010; current version published July 16, 2010. This work was supported in part by a grant from Xerox Corporation and in part by a grant from New York State Office of Science, Technology & Academic Research (NYSTAR) through the Center for Electronic Imaging Systems (CEIS). Parts of this work were presented at the 2008 IS&T/SPIE Electronic Imaging Symposium and at IEEE ICIP 2008. The associate editor coordinating the review of this manuscript and approving it for publication was Dr. Stefan Winkler.

O. Bulan is with the Department of Electrical and Computer Engineering, University of Rochester, Rochester, NY 14627 USA (e-mail: bulan@ece.rochester.edu; bulanorhan@gmail.com).

G. Sharma is with the Electrical and Computer Engineering Department and the Department of Biostatistics and Computational Biology, University of Rochester, Rochester, NY 14627 USA (e-mail: gaurav.sharma@rochester.edu; g.sharma@ieee.org).

V. Monga was with Xerox Research Center, Webster, NY 14580 USA. He is now with the Department of Electrical Engineering, Pennsylvania State University, University Park, PA 16802 USA (e-mail: vmonga@engr.psu.edu).

Color versions of one or more of the figures in this paper are available online at http://ieeexplore.ieee.org.

Digital Object Identifier 10.1109/TIP.2010.2046795

[1]The halftoning is actually performed prior to the physical printing process. In our description, we will either include the halftoning within the printing step or consider it as a separate preprocessing stage. Thus, when we refer to the print-scan process, it may include or exclude the halftoning step. Our meaning will, however, be clear based upon context.

halftoning technique employed in electrophotographic and lithographic printing systems. In addition to the distortion introduced in the binarization process, fidelity requirements for the halftone images, local geometric distortion inherent in printing, global rotation and scaling introduced in the scanning process, variations in absolute device responsivity for the printer-scanner combination, and noise due to other causes pose significant challenges in our application scenario. We address these challenges, while maintaining the requirements of automated detection and high capacity, by proposing a novel framework that incorporates several innovations. First, we perform the embedding jointly with the halftoning, emphasizing image fidelity in the process and, if necessary, sacrificing the capability to recover individual data values from even the digitally generated binary halftone images. We accomplish this by utilizing analytical halftone threshold functions that are independently modulated within each halftone cell based upon a corresponding data value to be embedded within the cell. In halftone cells where the image fidelity requirements permit flexibility, by our design, the modulation generates elliptically shaped halftone dots whose orientations are determined by the data value embedded in the corresponding cell. In other halftone cells, the effect of the modulation is dominated by the image fidelity mandates, resulting in erasures and errors in the data embedded in the digital halftone images, even prior to printing. To overcome these and other sources of errors, we propose a suitable data detection and error control methodology that uses image moments as detection statistics for inferring dot orientation within individual cells and an image gray-level dependent characterization of the print-scan channel that enables effective soft decoding. In order to recover from the deleterious effects of geometric distortion inherent in the print-scan process, we also propose a useful two stage methodology that exploits the periodic halftone structure to recover from global rotation and scaling and additionally incorporates a novel decision directed synchronization technique that allows us to overcome local geometric distortion introduced in the printing process.

In the existing literature, several techniques have been presented for data hiding in printed images. The methods proposed for data hiding in hardcopy images can be grouped into two main categories. The methods in the first category embed data in a contone (e.g., 256-level gray scale) image using a method intended to achieve robustness to a generic print-scan process [11], [23]–[25]. These methods do not adapt to the particular channel characteristics in the embedding stage and therefore, the print-scan channel appears as a rather severe distortion that adversely affects detection robustness and data rates. Applications for these methods are therefore, limited to low capacity applications such as document authentication and integrity verification. Methods in the second category exploit particular printing characteristics (e.g., halftoning) for embedding and, hence, offer greater potential for embedding. A majority of the pre-existing methods in the later category rely on visual detection of the embedded data [9], [12], [15], [26], [27]. These methods embed text or other visual patterns that are imperceptible in the printed images but become apparent in the detection process, e.g., by overlaying a predesigned binary pattern on the hardcopy print. While this is useful for some applications such as document authentication, copyright management and entertainment/novelty imaging, other applications such as meta data embedding, document tracking in workflows and encrypted data embedding can only be enabled by automated data recovery. A joint halftoning and watermarking scheme that allows automated detection was proposed in [28]. The method is applicable for dispersed dot halftone printing systems and embeds a single spread spectrum watermark (0-bit watermark) by employing a search over several candidate halftone patterns, in a manner similar to direct binary search [29]. The search makes the method too slow for real-time printing applications. Real-time joint halftoning and embedding methods for high-rate information embedding in error diffused halftone images used in inkjet printers have also been proposed [30], [31]. Techniques that select from a plurality of dispersed dot (stochastic) screens [32] could also potentially be adapted for data hiding. Though practical, these schemes do not extend to the large volume of prints generated with clustered dot halftones on electrophotographic and lithographic printers—a gap that our work fills.

We also note that for halftone data hiding a number of methods have also been proposed that do not consider the print-scan channel or consider an ideal channel free from distortions [33], [34]. These methods are, however, not robust to the distortions inherent in the print-scan process and therefore, address the rather limited class of applications where halftone images are preserved and used in electronic rather than printed format. Alternatively, the idealized print models they assume, would apply at rather low resolution with attendant loss of image quality.

The rest of this paper is organized as follows. Section II describes the halftone print channel characteristics and motivates our data hiding scheme. In Section III, we introduce the proposed data hiding scheme via halftone orientation modulation. Section IV describes data recovery from scanned images and the probabilistic print-scan channel model. Channel coding to counter errors and erasures is described in Section V. Experimental characterization of the perceptibility of embedding distortions, and practically achievable embedding rates and bit error probabilities are presented in Section VI. Section VII highlights several key aspects of the proposed framework. Section VIII concludes the paper by summarizing our main findings.

II. Overview

Halftoning is widely used in most printers and constitutes the primary distortion for hardcopy data hiding. In this section, we therefore, summarize halftone data hiding channel characteristics and give an overview of the overall proposed scheme motivated by these characteristics. Fig. 1 illustrates a halftone data hiding and recovery process where the contone image $I(x,y)$ and the message $\mathbf{m}$ constitute the inputs to the encoder. The halftoning and embedding processes produce a halftoned image $I^h(x,y)$ that: (a) visually approximates the original image $I(x,y)$, and (b) carries the message data $\mathbf{m}$. The halftone image is then printed and the decoder attempts to recover the embedded data from a scan of the printed image. In practice, data embedding can be performed prior to, after, or concurrently with halftoning. In the first case, the halftone

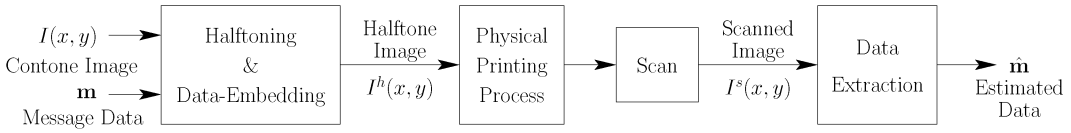

Fig. 1. Data embedding for the halftone print channel.

print channel appears as a rather severe distortion that hiding technique must overcome. If the embedding is performed after halftoning, on the other hand, ensuring acceptable image quality is challenging because the image is already in a binarized representation. Methods that perform embedding and halftoning jointly are, therefore, typically preferable when this is feasible.

Halftone data hiding channels exhibit several interesting characteristics.

1) The goal in halftone data hiding is to recover the embedded data from a scan of the printed image. As such, in most applications a malicious adversary is nonexistent. The "print-scan" channel and inadvertent distortions, however, already pose a significant challenge for data extraction.
2) Considering the set of visually pleasing halftone images that only satisfy the first of the two requirements outlined previously, some useful observations can be made about the halftone data hiding channel capacity. First, the discrete nature of the halftone process ensures that there are a large but finite number of halftoned images. From this large set, only a small subset will provide a perceptually acceptable representation of the original contone image. Even in the absence of any constraint for watermark detection the cardinality of this set defines a limit on the capacity of the halftone channel.
3) We also note that the capacity of the data-hiding channel can be bounded above by the entropy of the available halftone configurations. While this characterization is intractable for complete images, some useful observations can be made with regard to the local embedding capacity for different image regions. First observe that, in purely black and white regions of the cover image, the capacity is zero since there is only one configuration for the halftones in these regions. Furthermore, for regions with close to 50% halftone area coverage, again the capacity is rather small since the number of acceptable halftone configurations in these regions are small. For the specific case of clustered-dot halftones, typically only two differently phased checkerboard configurations are acceptable in the region of 50% area coverage and thus these regions have essentially a single bit capacity (over the relatively large regions that may have this area coverage).
4) The spatial variation in the contone image can also limit the available halftone configurations. In relatively smooth regions of the cover image, there is considerable flexibility in the choice of local halftone configuration yielding a higher upper bound on capacity. On the other hand, in the busy image regions, typically there is lesser flexibility in the choice of halftone configuration due to image fidelity considerations and concurrently a smaller capacity. In an extreme scenario, if the input image pixels assume random binary values, the halftone image is completely predetermined leaving rather limited flexibility for embedding.[2]
5) Based upon the preceding observations, informed embedding[3] for the halftone channel attempts to shape the spatial distribution of the embedded signal power to concentrate the power in smooth regions that are not close to critical gray-levels (i.e., shadows, highlights and 50% area coverage) since those regions provide considerable flexibility in the choice of the local halftone configuration. Thus, informed embedding for the halftone channel makes departure from conventional multimedia data embedding where watermark power is mostly concentrated in relatively busy regions [35].
6) In the absence of additional print-scan distortions, in smooth regions of the cover image, the halftone data hiding channel behaves like an erasure channel. For example, as indicated earlier, any data hidden in pure black and white regions will be erased even in the absence of any noise. In the presence of varying image content and print-scan noise, this leads to both errors and erasures at the receiver. In order to correct these erasures and errors, a solution based upon error and erasure correcting codes is required.

Motivated by these characteristics we propose a halftone data embedding method. Fig. 2 illustrates an overview of the overall proposed scheme. Here $\mathbf{m}$ denotes the message bits to be embedded and the cover image in which the data is to be embedded is denoted by $I(x,y)$. In order to allow error recovery at the receiver, the channel encoder introduces redundancy in the message producing the coded data $\mathbf{c}$. Using the cover image and the coded data, the operations of halftoning and data embedding are performed jointly in order to minimize the impact on image quality. The resulting image is printed and at the receiver a scan $I^s(x,y)$ of the hardcopy image is obtained. Detection statistics are obtained from the scanned image in the form of image moments $\boldsymbol{\sigma}$ and an estimate $\hat{g}$ of the local gray-level. These are utilized by the channel decoder to obtain an estimate $\hat{\mathbf{m}}$ of the transmitted message, either via soft decoding that utilizes a statistical model for the channel or via hard decoding. We describe the individual system elements in detail in the following sections.

III. Data Hiding via Halftone Orientation Modulation

The first system element in Fig. 2 consists of the channel encoder. In combination with the channel decoder this encoder provides error and erasure recovery functionality. Since the coding is motivated by the remainder of the channel, we defer a

[2]This in fact corresponds to post-halftone embedding.

[3]Note that we follow [18] to distinguish informed embedding and informed coding.

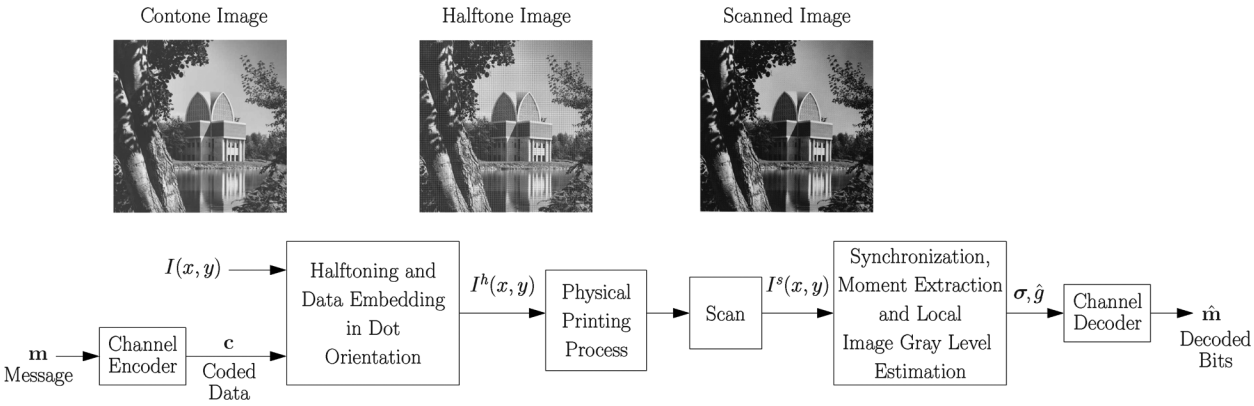

Fig. 2. Halftone data hiding framework with orientation-based embedding and error control coding.

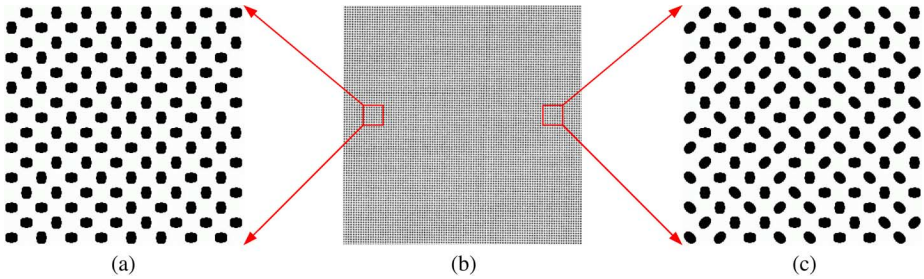

Fig. 3. Orientation based data embedding. (a) Binary dot orientation modulation (0/90°); (b) gray level halftone image; (c) 4-*ary* dot orientation modulation $(0/90^\circ/+45^\circ/-45^\circ)$.

discussion of the coding framework to Section V after we have described the basic data embedding and extraction methodology. In the rest of this section, we present our embedding method and detection of the embedded data from the halftoned image in the absence of "physical print-scan distortion."

A. Embedding Data in Halftone Orientation

We propose embedding data in clustered halftone dots by modulating the halftone-dot orientation. Specifically, we exploit the flexibility in the choice of halftone configuration by generating elliptically shaped halftone-dots oriented in various directions and embedding the data in the choice of a particular orientation. Fig. 3(a) shows the binary modulation in a constant image where dots are oriented in vertical and horizontal directions. Fig. 3(c) illustrates 4-*ary* case where a dot is oriented along horizontal, vertical and diagonal ($+/-45$ degree) directions, i.e., each orientation may be thought of as representing a 4-*ary* symbol value. As is the case for halftones in general, at typical printing resolution and viewing distances a human observer perceives the spatial average of the halftone as a uniform region as shown in Fig. 3(b).

The most common technique for generating clustered halftone dots is based upon screening [19], [36]. The contone image $I(x,y)$ is compared with a periodic threshold function $T(x,y)$. The threshold function is typically specified as a periodic array of threshold values for a given dot shape, printer addressability, and screen frequency. Designing the threshold function analytically, on the other hand, provides flexibility in choosing halftone parameters and other dot characteristics (e.g., phase [26]). Such a function is defined by Pellar [37], [38] for images taking values over the interval $[-1,1]$ as

$$T_0(x,y) = \cos(2\pi f_x x)\cos(2\pi f_y y) \tag{1}$$

where f_x and f_y represent the frequencies along the horizontal axis x and vertical axis y, respectively. Though Pellar threshold function offers flexibility in the choice of screen frequency, it has a limitation on the dot shape and can only produce symmetrically shaped halftone dots. We, therefore, modify the Pellar threshold function in such a way that it allows us to generate elliptical dots oriented along one of the orthogonal x and y axis.[4] The modified Pellar threshold function is expressed as

$$T(x,y) = \operatorname{sgn}\left(\cos(2\pi f_x x)\cos(2\pi f_y y)\right) \times \left|\cos(2\pi f_x x)\right|^{\gamma_x}\left|\cos(2\pi f_y y)\right|^{\gamma_y} \tag{2}$$

where γ_x and γ_y are parameters that control the dot shape and $\operatorname{sgn}(\cdot)$ denotes the signum function, i.e.,

$$\operatorname{sgn}(t) = \begin{cases} 1 & \text{if } t > 0 \\ 0 & \text{if } t = 0 \\ -1 & \text{if } t < 0 \end{cases}. \tag{3}$$

Fig. 4(a) shows $3-D$ representation of Pellar threshold function $T_0(x,y)$ and Fig. 4(b) denotes modified Pellar threshold function $T(x,y)$ for the case when γ_y is larger than γ_x. When γ_x and γ_y are equal, comparing a constant gray-level image with the threshold function $T(x,y)$ in (2) yields a dot that is symmetric about the x and y axes. Increasing the difference

[4]In actual practice, the threshold functions are linearized to correct for the printer response.

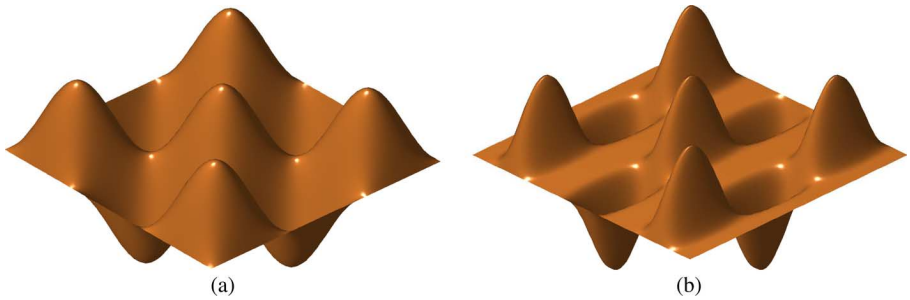

Fig. 4. Halftone threshold function orientation modulation. (a) Pellar threshold function $T_0(x, y)$ (b) modified Pellar threshold function $T(x, y)$ for $\gamma_y > \gamma_x$.

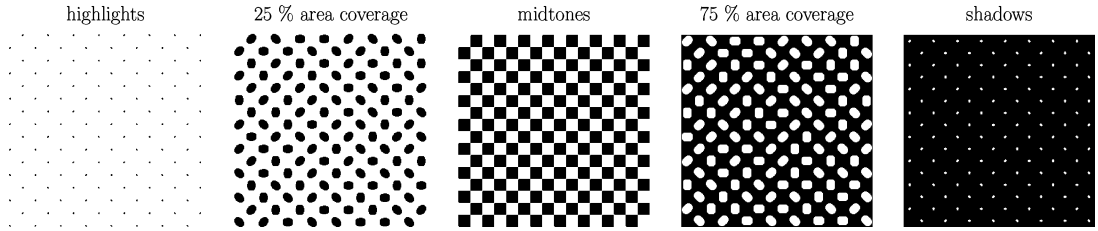

Fig. 5. Halftone data embedding via threshold function orientation modulation. Note that highlights, shadows and midtones encounter erasures.

between γ_x and γ_y on the other hand increases the ellipticity of the halftone-dot.[5] If γ_x is greater than γ_y, the dot is elliptical with a major axis oriented along vertical direction and when γ_y is larger the dot has its major axis oriented along the horizontal axis. The function $T_0(x, y)$ in (1) is periodic and for the 2-D tiling of the plane defined by the rectangular cells $[-(1/(4f_x)) + (m/f_x), (3/(4f_x)) + (m/f_x)] \times [-(1/(4f_y)) + (n/f_y), (1/(4f_y)) + (n/f_y)]$, $m, n \in Z$, $T_0(x, y)$ is uniformly zero at the cell boundaries. The same is true of $T(x, y)$ in (2) for any fixed γ_x and γ_y. As a consequence, if a data symbol is embedded in each of the afore-mentioned cells by modulating the values of γ_x and γ_y over the cell based upon the value of the data symbol, no discontinuities are introduced at the cell boundaries. Specifically binary embedding can be accomplished by defining $\Gamma_1 > \Gamma_2 > 0$ and modulating γ_x and γ_y over the mn^{th} cell based upon the corresponding bit b_{mn} for embedding

$$\gamma_x = \Gamma_2,\ \gamma_y = \Gamma_1, \quad \text{if } b_{mn} = 1 \text{ and} \tag{4}$$

$$\gamma_y = \Gamma_2,\ \gamma_x = \Gamma_1, \quad \text{if } b_{mn} = 0 \tag{5}$$

so that the "major axis" of the elliptical dot is oriented horizontally for bit values of 1 and vertically for bit values of 0. The dot-orientation modulation can be generalized to other directions by performing a rotation of the coordinate axes. Specifically, for a counterclockwise rotation of the coordinate axes by θ_i, x_i, y_i can be found as $x_i = x\cos\theta_i + y\sin\theta_i$ and $y_i = y\cos\theta_i - x\sin\theta_i$. θ_i represents the rotation angle of the coordinate system. For example, the coordinate transform with $\theta_i = 45°$ gives rise to a halftone dot oriented in $+45°$ direction when γ_y is larger than γ_x.

For M-*ary* embedding scenario, we set $\gamma_x = \Gamma_2$ and $\gamma_y = \Gamma_1$. The choice of γ_x and γ_y ensures that comparing a constant gray-level image with threshold function results in a dot oriented along horizontal direction in the absence of a coordinate transform. We select M different orientation directions as $\theta_i = 180(i-1)/M$ corresponding to symbols m_i, $i = 1, 2, \cdots, M$. In order to embed symbol m_i our embedding strategy performs coordinate transform with the angle θ_i. It then generates an elliptical halftone dot whose "major axis" makes an angle θ_i with the horizontal axis by comparing the contone image against the threshold function. The halftone image is then obtained as follows:

$$I^h(x, y) = \begin{cases} 1, & \text{if } I(x, y) \geq T(x, y) \\ 0, & \text{if } I(x, y) < T(x, y). \end{cases} \tag{6}$$

Our embedding method can be categorized as informed embedding since it incorporates the cover image knowledge, i.e., local gray-level in data embedding process. The local gray-level dependence of data embedding is illustrated in Fig. 5. While the dot orientation is noticeably distinguishable at gray-levels close to 25% or 75% area coverage, it is almost negligible in highlights, shadows and midtones. Data embedded at these gray-levels can be treated as erasures at the encoder and will be addressed by erasure and error correcting codes.

The spatial variation of embedding robustness depending upon the local cover image gray-level is also illustrated in the signal constellation of 4-*ary* orientation modulation shown in Fig. 6. In essence, the proposed modulation technique can be thought as an instantiation of both amplitude modulation (AM) and phase modulation (PM). The dot orientation is the parameter controlled by the modulation but the "robustness" of the dot orientation depends upon the local cover image gray-level. For example, in shadows, highlights and midtones the effective signal energy for the modulation is small whereas at gray-levels close to 25% and 75% area coverage it is significantly higher. At each gray-level, the dot orientation is quantized to modulate the message to be embedded which can be thought as phase

[5]At critical gray-levels i.e regions close to purely black, purely white or 50% area coverage ellipticity of the dot is negligible regardless of γ_x and γ_y and, hence, no variations in orientation are seen at these gray-levels despite the modulation.

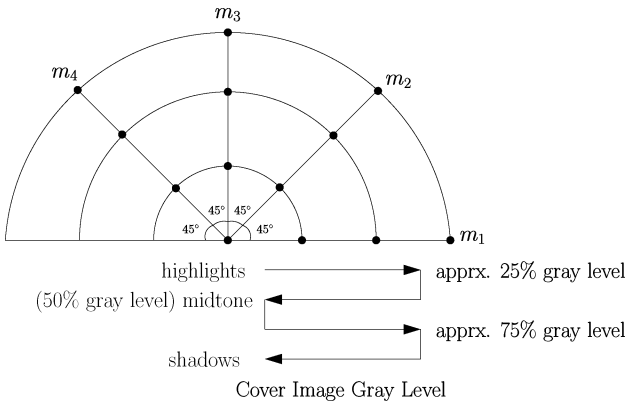

Fig. 6. Signal constellation for 4-*ary* orientation modulation with varying cover image gray-level.

modulation with an amplitude determined by the gray-level of the cover image.

B. Orientation Detection

We first consider detection of the dot-orientation in an idealized setting where the scanned image $I^s(x,y)$ directly corresponds to the halftone image without "physical print-scan distortion." In the perfectly synchronized and noiseless[6] scenario, we estimate the embedded data based upon statistically motivated image moments that capture orientation. We calculate image moments along every orientation direction utilized by the modulation process at the encoder,[7] obtaining an M dimensional feature vector $\boldsymbol{\sigma} = [\sigma_1, \sigma_2, \cdots, \sigma_M]^T$ from the high dimensional received signal corresponding to the scan image values $I^s(x,y)$ over pixel locations (x,y) lying in a halftone cell C. Specifically, within a halftone cell C, M image moments are calculated as

$$\sigma_i = \frac{\sum\limits_{x,y\in C} I^s(x,y)(u_i - \overline{u}_i)^2}{\sum\limits_{x,y\in C} I^s(x,y)} \quad \text{for all } i = 1, 2\cdots, M \quad (7)$$

where $u_i = x\cos\theta_i + y\sin\theta_i$ represents the abscissa in a coordinate system that is rotated counter-clockwise by an angle θ_i with respect to the image and $\overline{u}_i = (\sum_{x,y\in C} I^s(x,y)u_i)/(\sum_{x,y\in C} I^s(x,y))$ represents the corresponding coordinate for the center of mass of the cell (in the rotated space). In the two orientation modulation case with $\theta_1 = 0°, \theta_2 = 90°$, $(\overline{u}_1, \overline{u}_2)$ represents the center of mass over the halftone cell and (σ_1, σ_2) represents the image moments about the center of mass along x and y directions, respectively. In this case for uniform noncritical regions (see Sections II and III-A), $\sigma_1 > \sigma_2$ indicates a horizontally $(\theta_1 = 0°)$ oriented dot at $\sigma_2 > \sigma_1$ a vertically $(\theta_2 = 90°)$ oriented dot. More generally, the maximum moment indicates the dot orientation.

[6]Here we only assume the absence of physical print-scan distortion but the halftoning process inherently introduces some distortion in the embedded data that causes erasures and errors at the encoder as stated in Section III-A.

[7]If the halftone dots are perfect ellipses, it can be seen that the moment is maximum along the direction corresponding to the major axis of the ellipse.

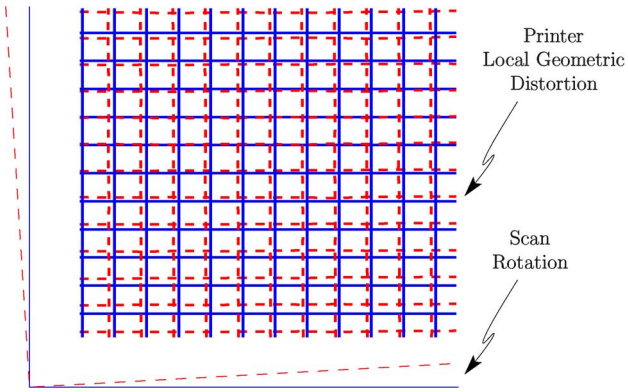

Fig. 7. Geometric distortion introduced by print-scan process.

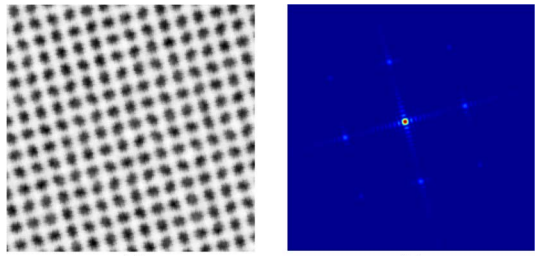

Fig. 8. Global rotation and periodicity estimation by frequency analysis: (a) cropped region from a scanned image with rotation; (b) Fourier transform of scanned image (zoomed-in view showing primary peaks).

Note that detection of the embedded data in the perfectly synchronized and noiseless case represents an oversimplified scenario. In essence, embedded data is exposed to interference from cover image and print-scan process that introduces geometric distortion and gray-level dependent noise.

IV. Data Recovery From Scanned Images

In this section, we describe the recovery of the embedded data after the halftone image goes through the print-scan process. The print-scan process introduces two kinds of distortion: 1) Global as well as local geometric distortions, and 2) noise introduced in printing/scanning. The receiver proceeds by first "undoing" (or compensating for) the geometric transformations in order to synchronize, and performs detection based upon the noise modeling of the resulting synchronized but noisy channel, which shows significant input gray-level dependence for the reasons we previously described.

A. Geometric Distortion Compensation

The effect of geometric print-scan distortions is illustrated in Fig. 7[8] using a sample print of a regular rectangular grid of lines. The solid (blue) lines show the input to the printer and the dashed (red) lines show the version rendered by the printer. The outer axes lines indicate the rotation between these introduced in the scanning process (over an 8 in $\times$ 8 in area). The inner finer grid shows a zoomed-in view (of an approx. 0.03 in $\times$ 0.03 in area) after compensation for the global rotation. The variation

[8]These plots in this figure, represent data from an actual printed and scanned image.

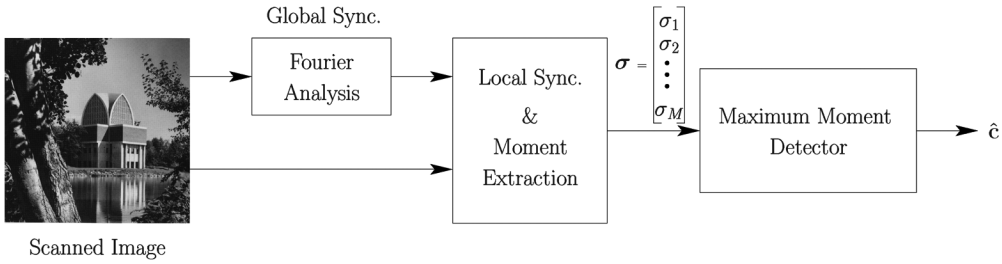

Fig. 9. Data extraction via maximum moment detection.

in the relative spacing between the dashed (red) lines illustrate the printer geometric distortion.[9]

As is well known in digital halftoning, clustered-dot halftones exhibit periodicity. This periodicity in turn can be exploited to compensate for the global geometric distortion. We note that this has been exploited in previous work as well [25]. The underlying principle is to approximate the halftone pattern as a 2-D impulse train, and look for corresponding peaks in the Fourier transform of the scanned image. Fig. 8(a) shows a zoomed-in view of a cropped region from a scanned image with rotation and Fig. 8(b) shows the Fourier transform of the image. In the Fourier transform, peaks corresponding to the halftone period are clearly seen. The location of these peaks provides a fairly accurate estimate of the global rotation introduced in the scanning as well as the periodicity of halftone-dots.

Local geometric distortions are more challenging. Due to local perturbations in the printing process, slight deviations may occur in the periodicity of the halftone dots. In order to compensate for these, we propose to use a technique analogous to decision directed synchronization, which is widely used in digital communications [40]. That is, when proceeding from top-to-bottom and left-to-right row-wise, we exploit the knowledge of previously decoded halftone dots (left and upper neighbors, specifically) to estimate the location of the halftone dot to be decoded next. Because of the periodicity of the halftoning process, the center of mass of the previous dot helps estimate the center of mass of the next halftone dot.

B. Maximum Moment Detection

We develop an intuitively motivated, albeit heuristic detection method called as *maximum moment* detection. As the name suggests, the detection strategy is based upon computing image moments along all candidate orientations and selecting the orientation corresponding to the dominant moment. That is, the index i^* of the detected orientation Θ_{i^*} is given as

$$i^* = \arg \max_{i=1,2,\ldots,M} \sigma_i. \tag{8}$$

Fig. 9 illustrates the data extraction process with the proposed maximum moment detection. First, global synchronization is achieved via Fourier transform analysis and then local distortion compensation and moment extraction are performed simultaneously. Finally, the orientation is detected based upon the rule in (8).

[9]In fact, the well known random-bending Stirmark attack [39] was originally created to emulate print-scan.

C. Channel Modeling and Maximum Likelihood Detection

The *maximum moment* detection criterion criterion in the previous subsection does not come with any optimality guarantees. Next, we develop a detection criterion which is optimal in the maximum likelihood (ML) sense. This entails a probabilistic modeling of the additive noise channel component of the print-scan process.

Before we describe our channel model, note that the detection accuracy inherently shows a strong dependence upon two aspects of the local cover image content: 1) local gray-level and 2) local entropy or variance. This is demonstrated in Fig. 10(b)–(g). These figures show zoomed versions of local regions in the scanned image. The original image in which data embedding was performed is shown in Fig. 10(a). The regions of the cover image, to which Fig. 10(b)–(g) correspond, are indicated by the alphabetic labels in Fig. 10(a).

Note first, that the regions where the cover image is purely white, no detection is possible as the only possible output binary halftone configuration is also pure white. As is intuitively clear, detection of embedded data is still hard when the image content is close to white as illustrated in Fig. 10(d). Likewise, in regions where the cover image is black, the halftone outputs are completely black allowing no detection. Finally, in mid-gray regions of the cover image that correspond to close to 50% halftone area coverage, the printed halftones take form a checker-board pattern [Fig. 10(e)] rendering orientation based detection useless. This impact of the gray-level of the cover image on the orientation modulation embedding channel can also be formalized in terms of a gray-level dependent characterization of the channel capacity that we have performed in related recent work [41].

Second, detection accuracy also varies significantly with the entropy of local cover image regions. If the image region is close to constant, well formed elliptical dots can be seen in the scan. However, for a high complexity region, halftoning maintains faithfulness to cover image detail and the extracted moments struggle to capture orientation information as is illustrated in Fig. 10(f) and (g).

To incorporate this peculiar dependence of the print-scan noise channel on the local cover image content, we propose a corresponding statistical model expressed in the form of the conditional density function $f_{\boldsymbol{\sigma}}(\boldsymbol{\sigma}|\Theta_i, g, v)$, where received (extracted) moments are conditioned on the local cover gray-level g, local cover image variance v and, orientations along different directions Θ_i, $i = 1, 2 \cdots, M$.

1) Marginalization Over Variance: We note that it constitutes a practically hard task to construct a channel model which

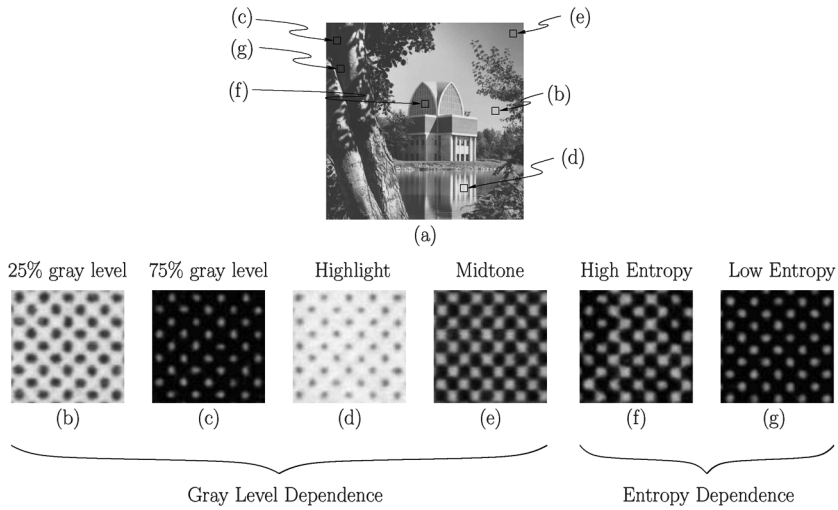

Fig. 10. Orientation based halftone data embedding via binary modulation.

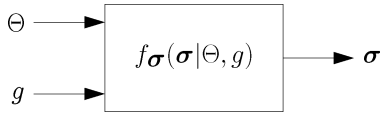

Fig. 11. Probabilistic modeling of the channel.

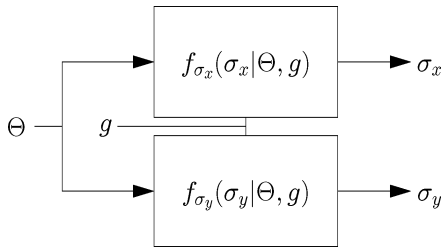

Fig. 12. Simplified probabilistic model of the binary orientation modulation channel.

includes conditioning on the local variance. This is because the estimated local image variance from a scan of the printed image can differ significantly from that of the original contone cover image. This is because the image is binarized through digital halftoning before printing.

In order to simplify the channel model, instead of $f_{\boldsymbol{\sigma}}(\boldsymbol{\sigma}|\Theta_i, g, v)$, we use only the marginal conditional density function $f_{\boldsymbol{\sigma}}(\boldsymbol{\sigma}|\Theta_i, g) = \int_0^\infty f_{\boldsymbol{\sigma}}(\boldsymbol{\sigma}|\Theta_i, g, v) f_v(v|\Theta_i, g) dv$ where $f_v(v|\Theta_i, g)$ shows the probability density function of variance v conditioned on the local gray-level g and orientations along different directions Θ_i, $i = 1, 2 \cdots, M$. We thus eliminate the channel dependence upon the local cover image variance v. Fig. 11 illustrates our resulting channel model.

2) Channel Characterization: We next focus on the mathematical characterization of the orientation modulation channel. In particular, we focus on the binary or two orientation case $f_{\sigma_x,\sigma_y}(\sigma_x, \sigma_y|\Theta_i, g)$ due to the limitations that practical printing systems introduce. The printing process inherently introduces directional distortion. When this distortion is coupled with arbitrary orientation modulation, unintended and undesirable variation may occur in the average gray-level of the printed halftone image. The variation in average gray-level gets harsher as the dot-orientation is quantized finer. Since the preservance of the average gray-level is the fundamental image fidelity criterion for halftone images, we limit the dot-orientation to two orthogonally oriented directions. While many sets of two orthogonal orientations are possible, for notational convenience we'll describe the modeling for vertically and horizontally oriented elliptical halftone dots.

Finding an analytical description for the multidimensional density function $f_{\sigma_x,\sigma_y}(\sigma_x, \sigma_y|\Theta_i, g)$, especially in the absence of physically inspired model, constitutes a hard task. To make the problem tractable, we assume conditional independence given by

$$f_{\sigma_x,\sigma_y}(\sigma_x, \sigma_y|\Theta_i, g) = f_{\sigma_x}(\sigma_x|\Theta_i, g) f_{\sigma_y}(\sigma_y|\Theta_i, g) \quad i = 1, 2. \tag{9}$$

We validate this assumption experimentally by observing the 2×2 covariance matrices of the received random vector σ_x, σ_y conditioned on Θ_1, Θ_2, for several gray-levels. In the Appendix we show that these matrices are close to diagonal justifying our assumption that σ_x, σ_y are approximately[10] conditionally independent. The simplified probabilistic model of the binary orientation modulation is shown in Fig. 12.

Based upon the aforementioned argument, it suffices to model the (marginal) conditional densities $f_{\sigma_x}(\sigma_x|\Theta_i, g), f_{\sigma_y}(\sigma_y|\Theta_i, g)$ of the observed moments σ_x, σ_y. For tractability, we further approximate these conditional densities by parameterizing them in terms of the exponential power density family [42] given by

$$f_X(x) = \frac{1}{2k\Gamma\left(1 + \frac{1}{l}\right)} \exp\left(-\left|\frac{x - \mu}{k}\right|^l\right) \tag{10}$$

where μ is the mean, and k and l are the scale and shape parameters of the distribution. For $l = 1$ the density corresponds to the Laplacian distribution and for $l = 2$ it becomes the Gaussian distribution with variance $k^2/2$. We estimate

[10]Zero covariance across the off-diagonals guarantees uncorrelatedness and not independence. Hence, we use the term approximately.

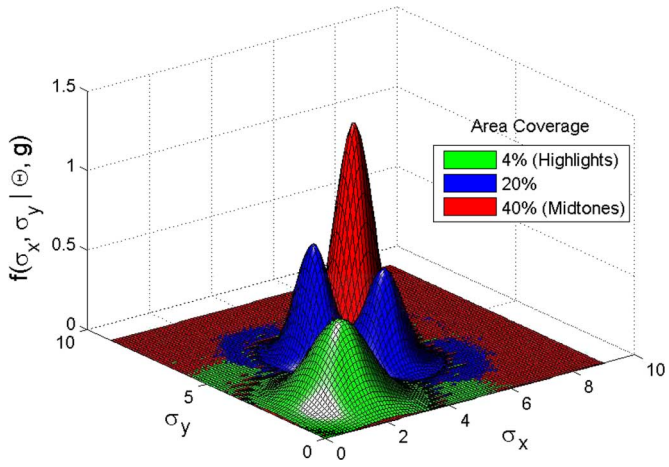

Fig. 13. Statistical channel conditional distributions for three different graylevels.

the distribution parameters from the experimental data by using an ML estimator.[11] For our experimental set-up (see details in Section VI), Fig. 13 illustrates the statistical channel conditional distributions in regions with requested halftone coverage corresponding to highlights (4%), midtones (40%), and a level approximately midway between these (20%) that is embedding friendly. For the embedding friendly level, the distributions for two orthogonal modulated halftone dot orientations are well-separated from each other, but they overlap significantly in highlights and midtones, which indicates that the channel model captures the graylevel dependence of the halftone modulation data hiding channel.

3) ML Detection: Based upon the probabilistic channel model, an ML detector is constructed as

$$\Theta^* = \arg\max_{i=1,2} f_{\sigma_x,\sigma_y}(\sigma_x,\sigma_y|\Theta_i,g) \tag{11}$$

$$= \max_{i=1,2} f_{\sigma_x}(\sigma_x|\Theta_i,g) f_{\sigma_y}(\sigma_y|\Theta_i,g). \tag{12}$$

Fig. 14 summarizes the maximum likelihood detection based upon exploiting the probabilistic channel model.

V. Channel Coding and Decoding for Erasure and Error Correction

As already noted in Section III-A, certain critical gray-levels (pure white, black, 50% gray and near-by intensity levels) are ill-suited for embedding/detection and introduce erasures at the encoder. Furthermore, interference from the cover image and other print-scan distortions cause additional errors and erasures. To realize a practical system, we therefore employ error correction codes (ECC). We consider two code families, viz. convolutional codes and Repeat Accumulate (RA) codes [44], [45].

A. Coding With Convolutional Codes

The motivation for the choice of convolutional codes is twofold. The first reason is good codes with low/moderate complexity are known for a variety of rates [46], [47]. The second reason is that the merit of the probabilistic channel model can be clearly demonstrated for these codes by contrasting soft and hard decoding.

Convolutional codes are well known and detailed descriptions of these may be found in standard digital communication texts [40], [48]. A convolutional code is generated by passing the binary information sequence to be transmitted through a linear finite-stage shift register that utilizes k input bits at each step, along with the available history of past inputs, to generate n encoded bits, yielding a code rate of k/n. The wide variety of convolutional codes [46], [47] with many different code rates and constraint lengths make them a particularly attractive choice for illustrating different aspects of system performance.

B. Repeat-Accumulate (RA) Coding

The choice of RA codes was motivated by their simplicity, flexibility in choice of rate, and near-capacity performance for additive white Gaussian noise (AWGN) and erasure channels [44], [45]. Additionally, these codes handle the erasures at the encoder rather well, and like convolutional codes provide flexibility to vary the rate through a change of the repetition parameter. As shown in Fig. 15, an RA encoder is composed of three stages. An information block of length L is repeated n times, scrambled by a random interleaver of size nL, and then encoded by a rate 1 accumulator. The rate of the RA code is $1/n$ and is readily changed simply by changing the repetition factor n.

C. Channel Decoding

Maximum likelihood decoding of convolutional codes can be achieved by the Viterbi algorithm [49] which allows for both hard and soft decoding. Approximate maximum aposteriori probability (MAP) decoding for RA codes is accomplished using belief propagation [50] for iterative decoding.

1) Hard Decoding: The hard decoding process is a concatenation of "ML detection" as described in Section IV-C followed by classical error correction decoding. This is illustrated in Fig. 16. The ML detector makes a decision on the embedded data by estimating the local gray-level and the image moments over each halftone cell and using these estimates in the probabilistic channel model according to (12) to estimate the bit embedded in the cell. Error correction decoding is then performed by using the resulting estimates of the encoded bits, collectively.

2) Soft Decoding: As is evident here, and also well known from classical communications, hard decoding does not fully exploit the knowledge of the probabilistic channel model. Soft decoding can offer performance improvements by propagating the knowledge of the channel as a soft measure to the error correction decoder. This is illustrated in Fig. 17. For both convolutional and RA codes, the soft measure used in decoding is the log likelihood given by

$$\gamma = \log f_{\boldsymbol{\sigma}}(\boldsymbol{\sigma}|\Theta_i,\hat{g}) \quad \text{for } i = 1,2\cdots,M \tag{13}$$

where $\boldsymbol{\sigma}$ contains the image moments along different directions computed within the halftone cell as indicated in Section IV and $\hat{g}$ is the estimate of the local gray-level obtained as the average of the pixel intensity values within the halftone cell.

[11]When only mixtures corresponding to randomly embedded values are observed, the Expectation-Maximization algorithm [43] may be used instead.

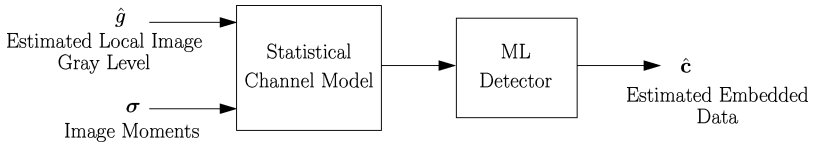

Fig. 14. ML detection incorporating the statistical channel model.

Fig. 15. Encoder for RA codes.

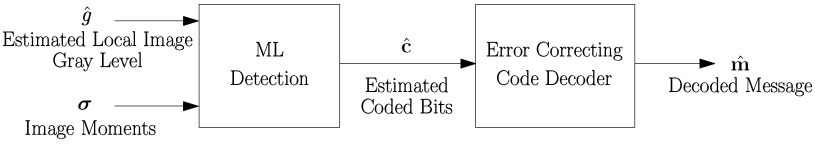

Fig. 16. Hard decoding.

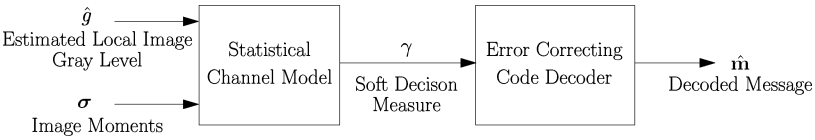

Fig. 17. Soft decoding.

VI. Experimental Results

We implemented our proposed halftone image data hiding scheme and the associated decoding method and evaluated its performance experimentally utilizing a print-scan channel consisting of a electrophotographic printer and a desktop scanner. A randomly generated bit stream was used as the message data in our experiments. This data was encoded utilizing the encoder for the error correction code in consideration (either convolutional or RA). The resulting coded data and a target cover image served as the input to a module which jointly performed the halftoning and the data-embedding operations. In our work, we utilized an orthogonal clustered dot halftone tiling with a frequency of 75 cells per inch and a 45° orientation[12] and choose $\Gamma_1 = 2$ and $\Gamma_2 = 1$ for modulating the halftone spot. The resulting halftone image (with data embedded in the orientation) was printed on the electrophotographic printer, which had an addressability of 2400 dots per inch (dpi). The resulting print was scanned on a desktop scanner with a 1200 dpi resolution. Global synchronization was performed by utilizing the periodic grid of the halftones and geometric distortion in the printing process was accounted for via decision directed local synchronization (as described in Section IV-A). Post-synchronization, the estimate $\hat{g}$ of the average gray-level in the halftone cell was obtained and image moments along the potential embedding directions, were computed as indicated in Section III-B.

The print-scan channel was first characterized by utilizing a set of training images, from which the parameters for the statistical channel model of Section IV-C were obtained. The system performance was then evaluated by utilizing an independent corpus of twenty-four test images as the contone cover images. The images were chosen to represent diversity of content and are shown in Fig. 21 for the purpose of illustration. The printed size of each image was 8×8 inches and a total of 414,960 symbols were embedded in the resulting printed image.

In the following, we present the results of experiments addressing the two main requirements of data hiding viz. perceptibility of the embedding changes and error performance for data embedding and decoding, with and without the error control coding.

A. Perceptibility of Embedding Changes

We conducted a psychophysical experiment to evaluate the impact of orientation modulation on the printed image quality.[13] From among the images in Fig. 21, fifteen contone images with varying content were selected. For each image, a pair of halftone prints was generated, with one print incorporating the orientation modulation based data embedding and the other print having no orientation modulation. The latter print utilized the Pellar halftone spot function ($\gamma_x = \gamma_y = 1$ in (2)) and linearization of the halftones was performed independently for the two cases. Fifteen observers were then engaged in a pairwise comparison task, where each subject was asked to indicate his/her preference for one of the prints in a pair after viewing the prints from viewing distance of approximately 10 inches. The order

[12]The orientation of the halftone tiling [19, Chap 6] is not to be confused with the orientation of the halftone dots used for embedding.

[13]Note that common image quality measures are of little assistance in our setting. Particularly, mean-squared error metrics for the embedding distortion, that are often used for the multimedia embedding scenario are less meaningful in the halftone channel, where it is well known that the pixel-wise thresholding provides the lowest mean squared error but rather poor visual quality.

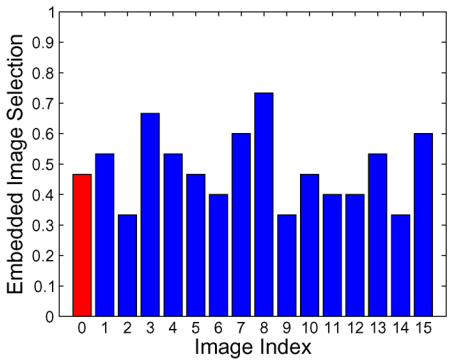

Fig. 18. Pairwise comparison results over each individual print pair (image indices 1–15) and averaged over the collection of 15 images (image index 0). The bar heights indicate the fraction of times the print with the embedded data is prefered (by observers) over the print with no embedding.

of the prints and their arrangements in pairs were randomized prior to presentation in order to eliminate systematic bias due to other factors. The results of the experiment are summarized in Fig. 18 where the heights of the bars indicate the fraction of observers that indicated a preference in favor of the print with the orientation modulation based embedding. The results for each individual image and the averaged results over the full set of images are both included in the figure. The average results indicate that observers preferred the prints with the orientation modulation 47% (7/15 th) of the time on average. That is, roughly half the time the print with the data embedded was judged preferable by the observers, thereby implying that the embedding causes almost no perceptual degradation.

Due to the small number of observers, a greater variability is seen in the results for individual images though they are still in agreement with our conclusion. The results demonstrate that our method of data embedding concurrently with halftoning meets its goal of maintaining a high image quality despite a relatively high data embedding rate (of one bit per halftone cell).

B. Detection Performance Without Error Correction

The performance of the orientation based halftone data embedding and the image moment based detection was first evaluated over the print-scan channel in the absence of error control coding.[14] For this purpose, we evaluate symbol error rates for the "modulation subsystem" of our framework, i.e the symbol error rates for a detector operating on the image moments at the output of the "synchronization, moment extraction and local image gray-level estimation" block in Fig. 2 when comparing against the symbols that form the input for the "Halftoning and data embedding" block (in Fig. 2). Furthermore, we first consider the performance for spatially constant (viz. uniform gray-level) images as a function of gray-level and then consider the performance for more typical images encountered in practice.

For the case of embedding using two orientations, (i.e., one bit per halftone cell) Fig. 19(a) plots the practically observed bit error rate (BER) as a function of gray-level. Plots are provided for both maximum moment detection and ML detection using the statistical channel model. Not surprisingly error rates are lower when ML detection is employed. Remarkably though the improvements are small indicating that the, intuitively motivated and fast, maximum moment detection does not sacrifice optimality with respect to ML detection. We similarly obtain symbol error rates (SER) for 4-ary modulation, or embedding using four orientations. These are plotted in Fig. 19(b). Because we characterized the channel only for the binary case,[15] here only the results corresponding to the maximum moment detector are reported. As is evident from both Fig. 19(a) and (b), data embedded in gray-levels ranging from 30 to 115 and from 135 to 215 can be recovered with a reasonable BER and SER. (A gray-level of 0 denotes black while 255 represents white.) This variation of BER/SER as a function of gray-level shows the dependence of the print-scan channel on the input gray-level. Further, the results corroborate intuition: gray-levels close to pure white, pure black and midtones (approximately 50%) do not allow halftone configurations that are distinguishable at the receiver and therefore exhibit high error rates (close to random guessing performance in each of the cases).

Next, we similarly obtain error rates in the case of embedding in more "realistic" images. We use four images from the Kodak database [51]: a) Eiffel (tower), b) Fraumunster (cathedral), c) Schwangau (church), and d) Windmill, which are shown in Fig. 21(a)–(d), respectively. For image quality reasons, binary orientation modulation was used for embedding. We also examine the impact of scanner resolution in this setting. Table I summarizes the BER performance for scan resolutions ranging from 600 to 1500 dpi. From the results, we see that our choice of 1200 dpi is adequate: higher resolutions offer minimal benefit whereas lower resolutions increase the BER significantly. For a 1200 dpi resolution, we also compare the maximum moment and ML detection modes in Table I. As before, the use of ML detection offers an improvement, albeit a small one.

C. Detection Performance With Error Correction Coding

As indicated earlier, convolutional codes and RA codes were utilized in our experiments. In each case we used a rate $1/n$ codes for different values of n. A randomly generated message was encoded using the suitable encoder in each case and the corresponding decoder was employed at the receiving end.

1) Performance Using Convolutional Codes: Rate $1/n$ convolutional codes were used for $n = 2$, 4, 5, 6, 7, 8, 10, 12, and 14. The codes used in our experiments are among the best codes known with low constraint lengths [46], [47]. Fig. 20 shows the hard and soft decoding BER results as a function of code rate for two sample images from the Kodak database [51]. From the figure, it is evident that soft decoding based upon the print-scan channel model significantly improves the error correction decoder performance yielding lower BERs than the hard decoding. The BER values are not exceptionally low because convolutional codes are not well-suited for the compensation of the erasures that occur at critical gray-levels though they do

[14]This step also required in order to estimate appropriate parameters for the error control coding scheme.

[15]The conditional independence assumption is hard to justify in the 4-ary case which in turn makes channel modeling considerably more difficult.

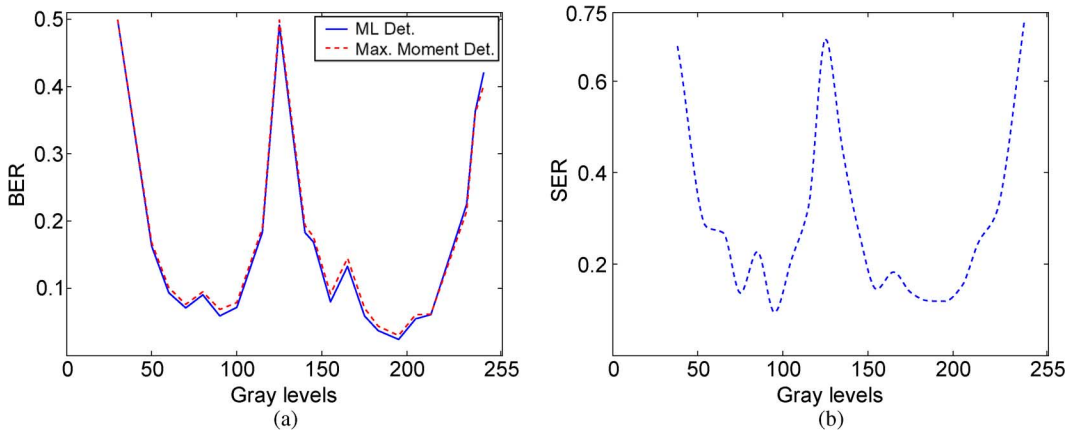

Fig. 19. Symbol error rates for the orientation modulation and detection subsystem over constant gray-level images as a function of gray-level: (a) binary modulation with ML (solid line) and maximum moment (dashed line) detection, (b) 4-*ary* modulation with maximum moment detection.

TABLE I
BER PERFORMANCE ACROSS FOUR IMAGES FROM THE KODAK DATABASE [51] FOR DIFFERENT SCANNER RESOLUTIONS

	BER				
	Maximum Moment Detection				ML Detection
Scanner Res.	600 dpi	900 dpi	1500 dpi	1200 dpi	1200 dpi
Eiffel	0.2603	0.1467	0.0575	0.0901	0.0763
Fraumunster	0.3126	0.2418	0.1419	0.1591	0.1508
Schwangau	0.3112	0.2355	0.1391	0.1639	0.1440
Windmill	0.3295	0.2544	0.1919	0.1944	0.1819

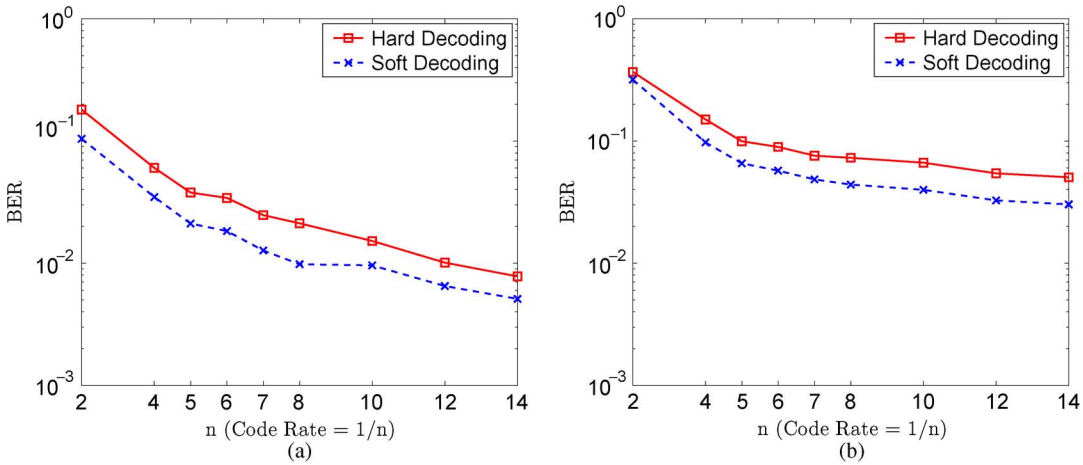

Fig. 20. Bit error rates obtained with rate $1/n$ convolutional codes as a function of n. With soft and hard decoding: (a) for Eiffel tower image [Fig. 21(a)], (b) for Schwangau church image [Fig. 21(c)].

serve to clearly demonstrate the value of our statistical channel modeling.

2) Performance Using RA Codes: In order to determine (operational) error-free embedding rates achieved by our method, we employ RA codes that perform near capacity in AWGN and erasure channels [45] and are therefore well suited to our scenario where cover image dependence can cause erasures and errors.

We evaluate the performance over several images with varying content as illustrated in Fig. 21. Because the print-scan channel exhibits a strong dependence upon the cover image content, we varied data rates to be embedded so as to achieve error free decoding. In each case, we were able to successfully extract the embedded data from the scans of the images. We determine that a code rate of 1/4 allows for error free decoding for images shown in Fig. 21(a)–(t).[16] This rate therefore provides an empirical lower bound on data hiding capacity, that is 0.25 bits per halftone cell.

VII. DISCUSSION

Several aspects of our framework are worthy of additional remarks.

[16]For images shown in Fig. 21(u)–(x) a lower code rate of (1/5) is typically required. For all images the RA code gave a BER of 0.01 when operating at a code rate of 1/4.

1) In halftone data hiding, embedding in orientation has the inherent advantage of low embedding distortion because a change of dot orientation does not change the average gray-level, which is the fundamental quantity that halftoning preserves. Furthermore, unlike methods that embed information in the image amplitude (or gray-level) the orientation embedding is relatively robust against gray-level modifications encountered in imaging systems such as the tone adjustment transformations that are commonly utilized in printing and scanning systems.
2) The error-free embedding rates achieved by our framework vary with printer/scanner resolution and screen frequency. Clearly the embedding rate of our method scales with the halftone frequency. The choice of screen frequency is normally correlated with the printer resolution since high frequency screens with low print resolution translate to inadequate number of graylevels [52] yielding poor image quality. Screens that offer a reasonable number of graylevels usually also offer sufficient flexibility in orientation modulation to enable data hiding. The scanner resolution should be chosen sufficiently high to ensure that adequate detail is captured for detecting the orientation modulation. Usually a scan resolution that is an order of magnitude higher than the haftone frequency is adequate though higher resolution can offer small improvements as shown by our results in Table I.
3) Our embedding strategy based upon halftone-dot orientation modulation has similarities with the data encoding method called DataGlyphs [6], [7]. The main difference between the proposed method and DataGlyphs is that the proposed method is a data hiding technique and concedes embedding robustness in favor of cover image fidelity in regions (i.e., high entropy regions and at critical gray-levels) where these two goals conflict with each other. DataGlyphs on the other hand, exercise the tradeoff in the other direction and therefore are closer to data-encoding rather than data hiding approaches. The second difference emerges from the detection algorithms. In contrast with our strategy of utilizing image moments for detection and error correction along with local and global geometric distortion compensation, DataGlyphs use a heuristic correlation based detection algorithm where the scanned image is binarized and then local blocks are correlated with possible binary patterns used for embedding after globally synchronizing with the scan. While this detection strategy compensates for global geometric distortions such as global rotation and scaling, it does not consider local geometric perturbations, which become more pronounced when smaller embedding cells are used to obtain higher rates. In our experimental setting, local displacements due to geometric distortions often exceed half the halftone cell size—scenarios under which a global approach to synchronization would fail catastrophically.
4) Though our framework offers excellent performance in terms of low distortion and high achievable (error free) rates, these benefits do levy a cost in terms of tradeoffs. The method is only applicable for clustered-dot halftoning methods and is not applicable for dispersed dot halftones that are extensively used in inkjet printing. Furthermore, since the embedding is performed jointly with halftoning, unlike methods that embed robustly in the contone domain and treat the print-scan process as (severe) distortion, the method relies on the ability to accurately control the printing of the cover image—which may be restrictive in some applications.
5) Our scheme can be categorized as informed embedding scheme [18] since it uses the host signal in the mapping from the message (binary symbol) to the mark (orientation) space giving priority to image quality in the process. Further, it is a quantization based embedding where the quantization is done in the various possible elliptical orientations, e.g., horizontal (0 degree), vertical (90 degree), diagonal ($+/-45$ degree) orientations etc. Despite the similarities, many characteristics of our proposed scheme make departures from classical results. As an example, in the proposed data hiding scheme, constant or low-entropy regions of the (contone) cover image are better suited for embedding and detection. The proposed method, unlike several of the pre-existing alternatives, achieves both robustness to electrophotographic-printing (and scanning) and automated data extraction.
6) Our methodology raises the bar for hardcopy data hiding methods, providing operational rates that compare favorably with 2-D barcodes. We demonstrate that in a typical image we can embed 202 bytes per square inch, which enables various high-rate hardcopy data hiding applications that would otherwise be infeasible [17]. This is roughly 1/7 th the rate for the Data Matrix 2-D barcode [3] and, in our estimate, at least two orders of magnitude higher than prior hardcopy data hiding methods for clustered-dot halftones that consider the print-scan channel as a post embedding distortion.

VIII. Conclusion

The framework we present in this paper is an effective solution for data hiding in images printed using clustered dot halftones, providing low distortion and automated data recovery with high capacity. Our method for embedding via orientation modulation during the halftoning process enables low distortion albeit at the cost of erasures and errors. A probabilistic characterization of the print-scan process that captures the channel dependence upon the cover image gray-level combined with suitable error control coding enables error free operation at high rates despite the many challenges in this application scenario. Our method makes departures from classical results in that constant and smooth image areas are better suited for embedding via our scheme as opposed to busy or "high entropy" regions. The error free embedding rates achieved by our scheme are higher than those achieved by prior methods for data embedding in clustered-dot halftone prints.

Appendix

In Section IV-C-2, we characterize a probabilistic model for the print-scan process which conditions received image moments on input orientations by assuming conditional independence for the multidimensional density functions. We validated this assumption by utilizing a measure that shows the dominance

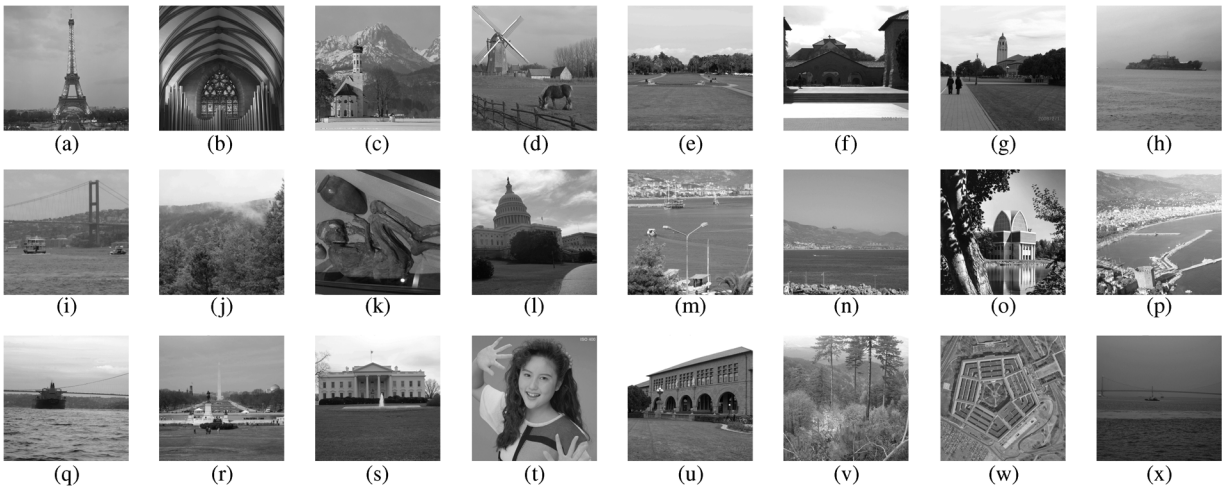

Fig. 21. Contone cover images used in the experiments.

of diagonal entries in the channel covariance matrices. For this purpose, over a collection of estimated 2×2 covariance matrices $\{C_i\}_{i=1}^{P}$ of the received random image moments σ_x, σ_y conditioned on Θ_1, Θ_2 for several gray-levels, we computed the measure $10\log_{10}(\sum_i ||diag(C_i)||_F^2 / \sum_i ||C_i||_F^2)$ where $||A||_F$ denotes the Frobenius norm of the matrix A and $diag(C_i)$ represents a diagonal matrix whose diagonal entries are identical to those in C_i. The above measure of the relative power of diagonal entries was evaluated over $P = 20$ uniformly spaced gray-levels, yielding a numerical value of -0.17 dB. This indicates that the covariance matrices are close to diagonal (the measure is 0 dB for the ideal diagonal case) and justifies our assumption.

REFERENCES

[1] O. Bulan, V. Monga, G. Sharma, and B. Oztan, "Data embedding in hardcopy images via halftone-dot orientation modulation," in *Proc. SPIE: Security, Forensics, Steganography, and Watermarking of Multimedia Contents X*, E. J. Delp, P. W. Wong, J. Dittmann, and N. D. Memon, Eds., Jan. 2008, vol. 6819, pp. 68 190C-1–68 190C-12.

[2] O. Bulan, G. Sharma, and V. Monga, "Adaptive decoding for halftone orientation-based data hiding," in *Proc. IEEE Int. Conf. Image Proc.*, Oct. 2008, pp. 1280–1283.

[3] Data Matrix Barcode FAQ & Tutorial Jan. 2008 [Online]. Available: http://idautomation.com/datamatrixfaq.html

[4] R. Villán, S. Voloshynovskiy, O. Koval, and T. Pun, "Multilevel 2D bar codes: Towards high capacity storage modules for multimedia security and management," *IEEE Trans. Inf. Forensics Security* vol. 1, no. 4, pp. 405–420, Dec. 2006 [Online]. Available: http://vision.unige.ch/publications/postscript/2006/TIFS-multilevel-2D-barcodes.pdf

[5] O. Bulan, V. Monga, and G. Sharma, "High capacity color barcodes using dot orientation and color separability," in *Proc. SPIE: Media Forensics and Security XI*, E. J. D., III, J. Dittmann, N. D. Memon, and P. W. Wong, Eds., Jan. 2009, vol. 7254, pp. 725 417-1–725 417-7.

[6] D. L. Hecht, "Printed embedded data graphical user interfaces," *IEEE Computer*, vol. 34, no. 3, pp. 47–55, Mar. 2001.

[7] D. L. Hecht, "Embedded data glyph technology for hardcopy digital documents," in *Proc. SPIE: Color Hard Copy and Graphic Arts III*, J. Bares, Ed., Mar. 2001, vol. 2171, pp. 341–352.

[8] J. Brassil, S. Low, N. Maxemchuk, and L. O'Gorman, "Electronic marking and identification techniques to discourage document copying," *IEEE J. Sel. Areas Commun.*, vol. 13, no. 8, pp. 1495–1504, Oct. 1995.

[9] K. T. Knox and S. Wang, "Digital watermarks using stochastic screens," in *Proc. SPIE: Color Imaging: Device Independent Color, Color Hardcopy, and Graphic Arts II*, G. B. Beretta and R. Eschbach, Eds., Feb. 1997, vol. 3018, pp. 316–322.

[10] Z. Baharav and D. Shaked, "Watermarking of dither halftoned images," in *Proc. SPIE: Security and Watermarking of Multimedia Contents*, P. W. Wong and E. J. Delp, Eds., Jan. 1999, vol. 3657, pp. 307–316.

[11] D. Corp, Digimarc Mediabridge 2000 [Online]. Available: https://www.digimarc.com/resources/docs/tech_papers/dmrc_media_bridge.pdf

[12] S. Wang, "Digital Watermarking Using Phase-Shifted Stoclustic Screens," U.S. Patent #6,252,971, 2001.

[13] C. Liu, S. Wang, and B. Xu, "Authenticate your digital prints with glossmark images," in *Proc. IS&T NIP20: Int. Conf. Digital Printing Technologies*, Oct. 2004, pp. 312–316.

[14] A. Mikkilineni, G. Ali, P. Chiang, G. Chiu, J. Allebach, and E. Delp, "Signature-embedding in printed documents for security and forensic applications," in *Proc. SPIE: Security, Steganography, and Watermarking of Multimedia Contents VI*, E. J. Delp and P. W. Wong, Eds., Jan. 2004, vol. 5306, pp. 455–466.

[15] G. Sharma and S. Wang, "Show-through watermarking of duplex printed documents," in *Proc. SPIE: Security, Steganography, and Watermarking of Multimedia Contents VI*, E. J. Delp and P. W. Wong, Eds., Jan. 2004, vol. 5306, pp. 670–684.

[16] R. L. de Queiroz, K. M. Braun, and R. P. Loce, "Detecting spatially varying gray component replacement with application in watermarking printed images," *J. Electron. Imag.*, vol. 14, no. 3, pp. 033 016,1–033 016,9, Jul. 2005.

[17] O. Bulan, G. Sharma, and V. Monga, "Application of high capacity data hiding in halftone images," in *Proc. IS&T's NIP 24: Int. Conf. Digital Printing Technologies*, Sep. 2008, pp. 787–791.

[18] I. Cox, M. Miller, and J. Bloom, *Digital Watermarking*. San Mateo, CA: Morgan Kaufmann, 2002.

[19] *Digital Color Imaging Handbook*, G. Sharma, Ed. Boca Raton, FL: CRC, 2003.

[20] H. R. Kang, *Digital Color Halftoning*. Piscataway, NJ: IEEE Press, 1999.

[21] P. Roetling and R. P. Loce, "Digital halftoning," in *Image Processing: Fundamentals and Applications*, E. R. Dougherty, Ed. New York: Marcel Dekker, 1994, ch. 10.

[22] K. T. Knox, "Digital halftoning algorithms and parameters," in *Proc. Int. Conf. LASERS*, 1990, pp. 619–625.

[23] S. Decker, "Engineering considerations in commercial watermarking," *IEEE Commun. Mag.*, vol. 39, no. 8, pp. 128–133, Aug. 2001.

[24] A. M. Alattar, "Smart images using digimarc's watermarking technology," in *Proc. SPIE: Security and Watermarking of Multimedia Contents II*, P. W. Wong and E. J. Delp, Eds., Jan. 2000, vol. 3971, pp. 264–273.

[25] K. Solanki, U. Madhow, B. S. Manjunath, S. Chandrasekaran, and I. El-Khalil, "'Print and scan' resilient data hiding in images," *IEEE Trans. Inf. Forensics Security*, vol. 1, no. 4, pp. 464–478, Dec. 2006.

[26] B. Oztan and G. Sharma, "Continuous phase modulated halftones and their application to halftone data embedding," in *Proc. IEEE Int. Conf. Acoustics Speech and Sig. Proc.*, May 2006, vol. II, pp. 333–336.

[27] T. Kimoto, "Hiding optical watermarks in hard copy images with reducing degradation of halftone quality," in *Proc. SPIE, Visual Communications and Image Processing*, Jul. 2003, pp. 1895–1904.

[28] D. Kacker and J. P. Allebach, "Joint halftoning and watermarking," in *Proc. IEEE Int. Conf. Image Proc.*, Sep. 2000, vol. II, pp. 69–72.

[29] M. Analoui and J. P. Allebach, "Model based halftoning using direct binary search," in *Proc. SPIE: Human Vision, Visual Processing, and Digital Display III*, B. E. Rogowitz, Ed., Feb. 1992, vol. 1666, pp. 96–108.

[30] N. D.-Venkata, J. Yen, V. Monga, and B. L. Evans, "Hardcopy image barcodes via block-error diffusion," *IEEE Trans. Image Process.*, vol. 14, no. 12, pp. 1977–1989, Dec. 2005.
[31] M. Fu and O. Au, "Data hiding watermarking for halftone images," *IEEE Trans. Image Process.*, vol. 11, no. 4, pp. 477–484, Apr. 2002.
[32] B. W. Kolpatzik and J. E. Thornton, "Image Rendering System and Method for Generating Stochastic Threshold Arrays for Use Therewith," U.S. Patent 5,745,660, Apr. 28, 1998.
[33] R. Li, O. Au, C. Yuk, S. Yip, and S. Lam, "Halftone image data hiding with block-overlapping parity check," in *Proc. IEEE Int. Conf. Acoustics, Speech and Signal Processing (ICASSP)*, 2007, vol. 2, pp. 193–196.
[34] B. K. Lien and B.-W. Shiue, "Hiding data in ordered dithering halftone images by bit interleaving," in *Proc. 3rd Int. Conf. Int. Information Hiding and Multimedia Signal Processing (IIH-MSP)*, Washington, DC, 2007, pp. 319–322.
[35] J. K. Su and B. Girod, "Power-spectrum condition for energy-efficient watermarking," *IEEE Trans. Multimedia*, vol. 4, no. 4, pp. 551–560, Dec. 2002.
[36] R. Ulichney, *Digital Halftoning*. Cambridge, MA: MIT Press, 1987.
[37] R. J. Pellar and L. Green, "Electronic Halftone Generator," U.S. Patent 4149183, 1979.
[38] R. J. Pellar, "Electronic Halftone Generator," U.S. Patent 4196451, 1980.
[39] F. Petitcolas, R. Anderson, and M. Kuhn, "Attacks on copyright marking systems," in *Proc. 2nd Int. Workshop Information Hiding*, Portland, OR, Apr. 1998, pp. 219–239.
[40] J. Proakis, *Digital Communications*, 4th ed. New York: McGraw-Hill, 2001.
[41] O. Bulan, G. Sharma, and V. Monga, "On the capacity of orientation modulation halftone channels," in *Proc. IEEE Int. Conf. Acoustics Speech and Signal Processing*, Las Vegas, NV, Apr. 2008, pp. 1685–1688.
[42] H. Stark and J. Woods, *Probability, Random Processes, and Estimation Theory for Engineers*, 2nd ed. Upper Saddle River, NJ: Prentice-Hall, 1994.
[43] J. Salojarvi and K. Puolamaki, "Expectation maximization algorithms for conditional likelihoods," in *Proc. 22nd Int. Conf. Machine Learning*, Aug. 2005, pp. 752–759.
[44] D. Divsalar, H. Jin, and R. J. McEliece, "Coding theorems for "turbo-like" codes," in *Proc. Allerton Conf.*, Monticello, IL, Sep. 1998, pp. 201–210.
[45] H. Jin, A. Khandekar, and R. McEliece, "Irregular repeat-accumulate codes," in *Proc. 2nd Int. Symp. Turbo Codes and Related Topics*, Sep. 2000, pp. 1–8.
[46] P. Frenger, P. Orten, and T. Ottosson, "Code-spread CDMA using maximum free distance low-rate convolutionalcodes," *IEEE Trans. Commun.*, vol. 48, no. 1, pp. 135–144, Jan. 2000.
[47] D. Daut, J. Modestino, and L. Wismer, "New short constraint length convolutional code constructions for selected rational rates," *IEEE Trans. Inf. Theory*, vol. IT–28, no. 5, pp. 794–800, Sep. 1982.
[48] T. K. Moon, *Error Correction Coding: Mathematical Methods and Algorithms*. Hoboken, NJ: Wiley, 2005.
[49] J. Forney and G. D. , "The Viterbi algorithm," *Proc. IEEE*, vol. 61, no. 3, pp. 268–278, Mar. 1973.
[50] J. Pearl, *Probabilistic Reasoning in Intelligent Systems: Networks of Plausible Inference*. San Mateo, CA: Morgan Kaufmann, 1988.
[51] Kodak Photo Database April 2008 [Online]. Available: ftp://ftp.kodak.com/ips/pub/Europe_Images/Europe-8bitTIFF/
[52] C. M. Hains, S. Wang, and K. T. Knox, "Digital color halftones," in *Digital Color Imaging Handbook*, G. Sharma, Ed. Boca Raton, FL: CRC, 2003, ch. 6.

Orhan Bulan (S'10) received the B.S. degree with high honors in electrical and electronics engineering from Bilkent University, Ankara, Turkey in 2006, the M.S. degree in electrical and computer engineering from University of Rochester, Rochester, NY in 2007, and is currently pursuing the Ph.D. degree candidate in the Department of Electrical and Computer Engineering at the University of Rochester.

He was with Xerox Webster Research Center, Webster, NY, during the summer of 2009 as a Research Intern. He is the recipient of best student paper award at the 2008 Western New York Image Processing Workshop organized by the Rochester Chapter of the IEEE Signal Processing Society. His research interests include signal processing, image processing, multimedia security, halftoning, and error correction coding.

Gaurav Sharma (SM'00) received the B.E. degree in electronics and communication engineering from Indian Institute of Technology Roorkee (formerly University of Roorkee), India, in 1990; the M.E. degree in electrical communication engineering from the Indian Institute of Science, Bangalore, India, in 1992; and the M.S. degree in applied mathematics and the Ph.D. degree in electrical and computer engineering from North Carolina State University, Raleigh, in 1995 and 1996, respectively.

From August 1992 through August 1996, he was a research assistant at the Center for Advanced Computing and Communications, ECE Department, NCSU. From August 1996 through August 2003, he was with Xerox Research and Technology, Webster, NY, initially as a member of research staff and subsequently at the position of principal scientist. Since Fall 2003, he is an Associate Professor at the University of Rochester in the Department of Electrical and Computer Engineering and in the Department of Biostatistics and Computational Biology. He is also the Director for the Center for Electronic Imaging Systems (CEIS), a New York state funded center for promoting joint university-industry research and technology development, which is housed at the University of Rochester. His research interests include multimedia security and watermarking, color science and imaging, genomic signal processing, and image processing for visual sensor networks. He is the editor of the *Color Imaging Handbook* (CRC, 2003).

Dr. Sharma is a member of Sigma Xi, Phi Kappa Phi, Pi Mu Epsilon, IS&T, and the signal processing and communications societies of the IEEE. He was the 2007 chair for the Rochester section of the IEEE and served as the 2003 chair for the Rochester chapter of the IEEE Signal Processing Society. He currently serves as the vice chair for the IEEE Signal Processing Society's Image and multidimensional signal processing (IMDSP) technical committee and is an advisory member of the IEEE Standing committee on Industry DSP. He currently serves as an associate editor the *Journal of Electronic Imaging* and in the past has served as an associate editor for the IEEE TRANSACTIONS ON IMAGE PROCESSING and the IEEE TRANSACTIONS ON INFORMATION FORENSICS AND SECURITY.

Vishal Monga (S'00–M'05) received the B.Tech degree in electrical engineering from the Indian Institute of Technology (IIT), Guwahati, in 2001, and the M.S.E.E. and Ph.D. degree in electrical engineering from the University of Texas, Austin in 2003 and 2005, respectively.

He is currently an Assistant Professor of Electrical Engineering at the main campus of Pennsylvania State University, University Park, PA. He was with Xerox Research from 2005–2009 and a Visiting Researcher at Microsoft Research in the summer of 2005. His research interests are broadly in multidimensional signal and image processing. He established the Information Processing and Algorithms Laboratory (iPAL) at Penn State. Current research themes in his lab include computational color and imaging, multimedia mining and security, and statistical learning for document processing, and robust decision problems on graphs.

Dr. Monga is a member of SPIE and IS&T. As a graduate student, he received the Texas Telecommunications Consortium fellowship for PhD studies and the Raymond Davis scholarship from IS&T in 2004. In 2008, he was awarded the Rochester Engineering Society Young Engineer of the Year. He currently serves as an Associate Editor for the IEEE TRANSACTIONS ON IMAGE PROCESSING and the SPIE *Journal of Electronic Imaging*.